A real-time prostate cancer detection technique using needle insertion force and patient-specific criteria during percutaneous intervention

K. Yan[a)] and T. Podder
Department of Radiation Oncology, Thomas Jefferson University, Philadelphia, Pennsylvania 19107

L. Li
Department of Pathology, University of Rochester, Rochester, New York 14627

J. Joseph
Department of Urology and Department of Surgery, University of Rochester, Rochester, New York 14627

D. R. Rubens
Department of Imaging Science and Department of Surgery, University of Rochester, Rochester, New York 14627

E. M. Messing
Department of Urology and Department of Surgery, University of Rochester, Rochester, New York 14627

L. Liao
Department of Radiology, Cooper University Hospital, Camden, New Jersey 08103

Y. Yu
Department of Radiation Oncology, Thomas Jefferson University, Philadelphia, Pennsylvania 19107

In this article, the authors present a novel real-time cancer detection technique by using needle insertion forces in conjunction with patient-specific criteria during percutaneous interventions. Needle insertion experiments and pathological analysis were performed for developing a computer-aided detection (CAD) model. Backward stepwise regression method was performed to identify the statistically significant patient-specific factors. A baseline force model was then developed using these significant factors. The threshold force model that estimated the lower bound of the cancerous tissue forces was formulated by adding an adjustable classifier to the baseline force model. Trade-off between sensitivity and specificity was obtained by varying the threshold value of the classifier, from which the receiver-operating characteristic (ROC) curve was generated. Sequential quadratic programming was used to optimize the CAD model by maximizing the area under the ROC curve (AUC) using a set of model-training patient data. When the CAD model was evaluated using an independent set of model-validation patient data, an AUC of 0.90 was achieved. The feasibility of cancer detection in real time during percutaneous interventions was established. © *2009 American Association of Physicists in Medicine*. [DOI: 10.1118/1.3213453]

I. BACKGROUND

Prostate cancer is the second leading cause of male cancer death in Europe and North America. In 2008, the National Cancer Institute (NCI) estimated that there would be 186 320 new prostate cancer cases in the United States, and about 28 660 persons would die from prostate cancer.[1] With the advent of prostate-specific antigen (PSA) screening, a majority of prostate cancers are diagnosed in the early stages. Of the various modalities of therapy, interstitial needle delivery of therapy such as brachytherapy is being increasingly used.

The needle-tissue interaction forces during percutaneous intervention have been a focus of research interests in the past several years.[2–10] For instances, needle insertion forces have been measured in tissuelike phantoms,[2,3] *ex vivo* human and animal organ samples,[4,5] *in vivo* animal experiments,[6] and *in vivo* prostate brachytherapy procedures.[7] The influ-ence of needle coating,[3] needle tip shape and insertion velocity,[8] and patient-specific factors[9,10] on the magnitude of insertion force was investigated as well. An extensive literature survey on needle-tissue interaction can be found in Ref. 11. The main objective of these studies was to predict or control the insertion force during penetration, so that more accurate needle placement and less tissue deformation can be achieved. The techniques in distinguishing different tissues (e.g., tumor vs normal tissue) by analyzing the needle-tissue interaction forces have been largely neglected.

Studies in the literature have shown that when tissues become diseased, changes in tissue composition, consistency, elasticity, and stiffness will occur. Some researchers analyzed prostate tissue *in vitro* and showed that there were variations in stiffness between tumor and normal tissue.[12] There were also variations between patients.[13] In general,

tumors resulting from abnormal and excessive cell division are harder than the normal healthy tissues. Therefore, tumors can be detected as hard lumps.[13] Sonoelastography, which is an ultrasound imaging technique relying on color Doppler information from the forced vibration of soft tissues where a hard inhomogeneity (such as a tumor) can produce a localized disturbance in the vibration pattern, has been developed to detect hard lesions in relatively soft tissue.[14–16]

In this paper, we present a real-time technique for cancer detection using the needle insertion forces and patient-specific criteria (e.g., patient age, ethnicity, prostate density, and PSA). To the authors' best knowledge, this is the first study in the reported literature to use the insertion force for cancer detection purpose. The proposed technique is developed as a candidate for robotic brachytherapy with real-time force sensing and intraoperative planning to achieve dose painting, so that the dose to malignant tumors can be escalated while nominal or even de-escalated dose may be delivered to nonsuspicious tissues.

II. MATERIALS AND METHOD

II.A. Needle insertion experiment using *ex vivo* human prostate

A total of 23 prostate samples were collected from patients who underwent radical prostatectomy in an Institutional Review Board (IRB) approved clinical study and with the patients' informed consent. Data of only 21 patients were used for analysis. Two patients were excluded from the present analysis due to either lack of patient-specific data or pathological data. Each sample was brought to the laboratory within 10 min of completing the surgical excision. The prostate sample was placed into a polyvinylchloride (PVC) phantom prepared beforehand [see Fig. 1(a)]. Two stabilization needles were used to mimic the scenario during the actual brachytherapy procedure. A set of 18-gauge diamond tip prostate brachytherapy needles (Mick Radio-Nuclear Instruments, Inc., NY) was used throughout the whole set of experiments. A six degree-of-freedom (DOF) robotic system equipped with a six DOF force-torque (*F-T*) sensor (Nano17®, ATI Industrial Automation, NC) was used to drive the needle into the prostate. The needle was inserted at a constant speed of 5 mm/s at ten locations in three zones that were defined empirically, i.e., peripheral zone (the posterior portion of the prostate), central zone (the inner portion of the prostate), and transitional zone (the area immediately surrounding the urethra), as shown in Fig. 1(b). Force-torque data were collected for analysis during the procedure. After the insertion experiment, the prostate sample was immediately sent to the surgical pathology laboratory for histological analysis. The prostate was sliced from apex to base at a thickness of 5 mm. In each histological slice, a total of ten locations around the needle insertion positions (one location for each needle) were identified and marked by the surgical pathologist (Li). The diagnosis was recorded in a pathology report describing the histological findings, which served as the ground truth in the following study for determination of the actual tissue characteristics (e.g., tumor or normal tissue).
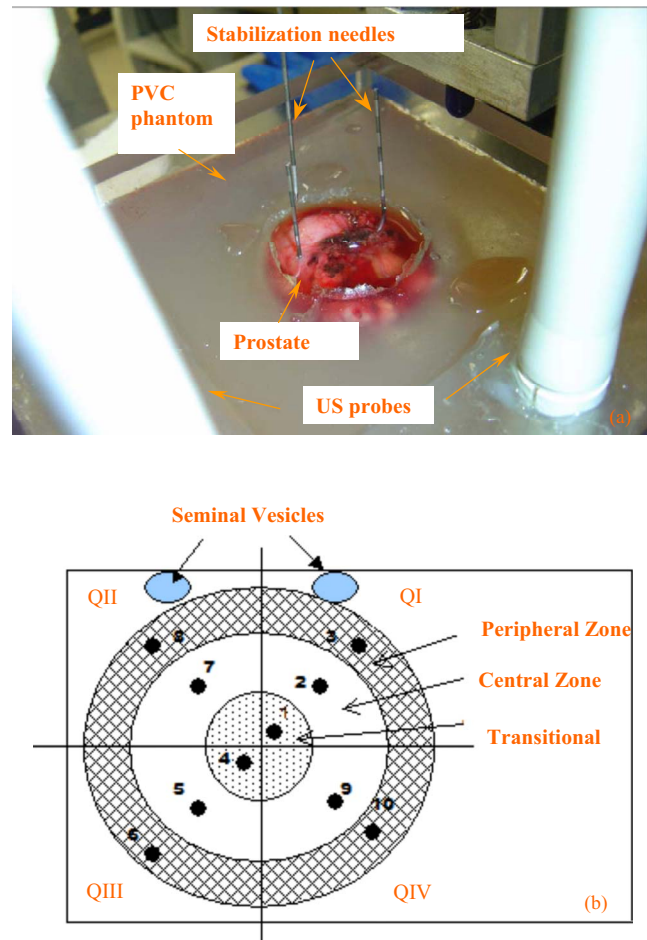
FIG. 1. Experimental setup: (a) Experimental platform; (b) distribution of needle insertions. The two ultrasound probes in the figure were used to capture the needle insertion procedure for postevaluation, i.e., tissue deformation, needle bending, etc.

II.B. Identification of statistically significant patient-specific factors

The patient-specific factors under consideration included patient age, ethnicity, body mass index (BMI), clinical stage, PSA, Gleason sum obtained from biopsy, prostate volume measured from the radical prostatectomy specimen, and prostate density calculated from measured prostate volume and weight. These factors may relate to the mechanical properties of the prostate tissue, thus influencing the insertion forces. Since the needle force was a function of insertion depth and may also be characterized by different zones, for simplicity, mean forces at the same insertion depth in the same zone were compared.

To determine the significance of these factors on the insertion force, backward stepwise regression was used: Starting with all the terms in the model, the least significant terms were sequentially removed until all the remaining terms were statistically significant. The *p values* that represent the significance of the factors and variance inflation factors (VIFs) that are a measure of the multicollinearity in a regression design matrix (i.e., the independent variables)[14] were evaluated for selection of the statistically significant factors. A *p*

value close to zero means that the parameters under testing are statistically significant and thus should be kept in the model. Here we chose $p=0.05$ as the cutoff value. For VIF, both 5 and 10 have been used in the literature as critical thresholds as a rule of thumb.[17] These VIF values correspond to R^2 (coefficient of determination) values of 0.8 and 0.9, respectively. Here considering the small size of the data set, 5 was selected; that is, if VIF was larger than 5, then multicollinearity was high. The Durbin-Watson number was also examined to detect autocorrelation in the model residuals. A value around 2 generally indicates that there appeared to be no autocorrelation, e.g., the models are properly specified and no significant information is left with the residuals. Considering the influence of the sample size and the number of statistically significant factors in the model, this statistic was compared with tabulated rejection values as shown by Durbin and Watson,[18] which were calculated based on those effects.

II.C. Tumor classification model optimization

The baseline model that estimates the mean force values in normal tissue can be represented using the equation as shown below,

$$F_b = \sum_{i=0}^{N} \beta_i X_i^{n_i}, \tag{1}$$

where X_i is the ith statistically significant patient-specific factor, β_i is the corresponding coefficient vector, n_i is the order of X_i, and N is the number of the statistically significant terms.

Thus the threshold force model that measures the lower bound of the cutoff force values in cancerous tissue can be represented as

$$F_t = F_b + \Delta, \tag{2}$$

where Δ, named "classifier," represents the estimated force difference between the cancerous tissue and the normal tissue. Forces equal to or higher than the threshold force will indicate the existence of cancerous tissue. Selecting different values of Δ has the effect of selecting different trade-offs between sensitivity and specificity. The area under the receiver-operating characteristic (ROC) curve (AUC), which aggregates the performance across the range of trade-offs (sensitivity and specificity) and is independent of the chosen classifier Δ, is of primary consideration for model optimization.

The optimization problem can be represented mathematically as

$$\max \mathbb{F}(\theta), \theta = (\beta, n) \in \Phi = \{g_i(\theta) \le 0, i = 0, 1, \dots, N_c\}, \tag{3}$$

where $\mathbb{F}$ represents objective "AUC," which can be calculated by integrating the area under the ROC curve. Here we define bounds or constraints to the parameters based on *a priori* information to improve the search efficiency. For example, if the relationship between certain statistically signifi-
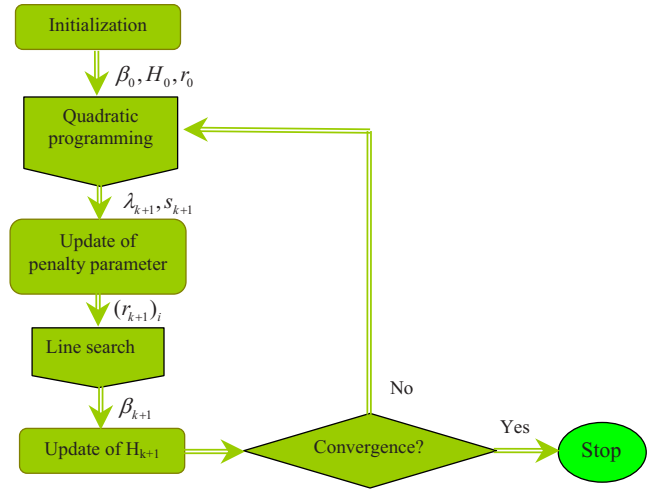

FIG. 2. Flow chart of SQP implementation.

cant factor and needle insertion force is known either empirically or from factorial study, a constraint will be set for that factor during optimization. Here, Φ is the feasible domain where the parameters satisfy all the constraints; $g(\theta)$ is the defined constraint function, and N_c is the number of constraints. Thus, this is a case of constrained optimization problem.

In constrained optimization, a commonly used method is to transform the problem into an easier subproblem that can then be solved and used as the basis of an iterative process. Some of the main techniques that have been proposed for solving constrained optimization problems are reduced gradient methods,[19] sequential linear programming and sequential quadratic programming (SQP) methods,[20] and augmented Lagrangians and exact penalty functions method.[21] The SQP method, which represents the state of the art in the nonlinear programming methods, has been used in this study. This method generates a quadratic programming (QP) subproblem by replacing the objective function with the quadratic approximation and the constraint functions with linear approximations, as shown in Eq. (4). The QP algorithm is used to calculate a feasible point and form a new iteration [Eq. (5)]. Then the Hessian matrix H in Eq. (4) is updated using the Broyden-Fletcher-Goldfarb-Shanno (BFGS) algorithm [Eq. (6)], which leads to the update of the subproblem in a new iteration until satisfactory convergence is achieved.[22] The detailed algorithm is illustrated in Fig. 2, in which r represents the penalty parameter that is updated using Eq. (7) in each iteration,

$$\min_{d \in \mathbb{R}^n} \frac{1}{2} d^T H d + \nabla \mathbb{F}'(\theta)^T d \quad \text{and} \quad \nabla g_i(\theta)^T d + g_i(\theta)$$
$$\le 0, \quad i = 1, \dots, N_c, \tag{4}$$

$$\theta_{k+1} = \theta_k + \alpha_k d_k, \tag{5}$$

$$H_{k+1} = H_k + \frac{q_k q_k^T}{q_k^T s_k} - \frac{H_k^T H_k}{s_k^T H_k s_k} \quad \text{with} \ \ s_k = \theta_{k+1} - \theta_k, \quad q_k$$

$$= \nabla \mathbb{F}'(\theta_{k+1}) + \sum_{i=1}^{N_c} \lambda_i \nabla g_i(\theta_{k+1})$$

$$- \left(\nabla \mathbb{F}'(\theta_k) + \sum_{i=1}^{N_c} \lambda_i \nabla g_i(\theta_k) \right), \tag{6}$$

$$r_i = (r_{k+1})_i = \max_i \left\{ \lambda_i, \frac{1}{2}((r_k)_i + \lambda_i) \right\}, \quad i = 1, \ldots, N_c, \tag{7}$$

where the matrix H is a positive definite approximation of the Hessian matrix of the Lagrangian function, $\mathbb{F}'$ is obtained by multiplying $\mathbb{F}$ with a negative sign, d is the search direction, α_k is a scalar step-length parameter determined by the line search procedure, so that a sufficient decrease in a merit function is obtained, and λ_i is the Lagrange multipliers. As a starting point, x_0 can be initialized to any vector that agrees with the constraints; H_0 is then a positive definite approximation to the inverse of the Hessian at x_0; r_0 can be initialized by[23]

$$r_{i0} = \frac{\|\nabla f(x)\|}{\|\nabla g_i(x)\|}, \tag{8}$$

where $\| \ \|$ represents the Euclidean norm.

III. RESULTS

III.A. Insertion force analysis

During the needle insertion experiment, the needle was inserted into the prostate from the apex to the base. At the beginning, the needle was accelerated to 5 mm/s by the robotic system. After the needle touched the prostate, the prostate first deformed and the force increased before the needle punctured through the capsule. The puncture point can be identified by the sudden drop in the insertion forces. After puncture, the needle moved inside the prostate until it quickly decelerated to stop. Figure 3 shows typical force profiles at the three zones in one of the patients. During the experiment, either failure of puncture (e.g., insertions 7 and 8) or late puncture (e.g., insertion 6) could happen due to the resistance of the prostate capsule or prostate translation or even rotation during the insertion procedure. In the entire set of experiments, a total of 59 insertions (28.1% of total insertions) were found to either fail in insertion into the prostate or could not be associated with the puncture points from both the force plot and the experimental records. Most of the insertion failures happened in the peripheral zone mainly due to the fact that the needle insertions in this zone induced the most unbalanced forces for the prostate, thus causing the prostate to rotate and increasing the difficulties of the needle insertion. This high failure rate would be greatly reduced in actual brachytherapy procedures since the *in vivo* prostate would be better supported from the surrounding connective tissues as compared to the prostate specimen setup during the experiment. In the transitional zone, there was a higher like-
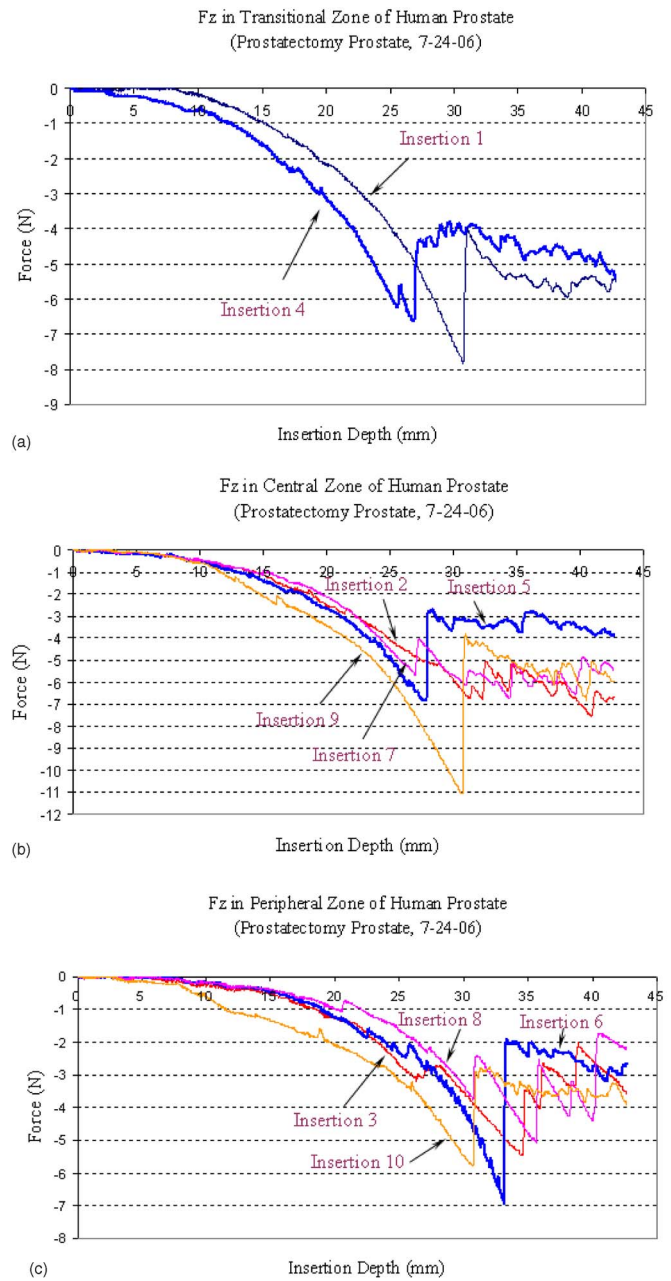

FIG. 3. Typical force profiles in (a) central zone, (b) transitional zone, (c) peripheral zone of the prostate.

lihood of encountering the urethra, which was relatively harder than the prostate tissue and could result in increased force, thus constituting great disturbance for force analysis. In some cases, the needles were even deflected when inserting into the urethra. Thus in the current study, we mainly focused on analyzing the forces in the central zone, where sufficient numbers of successful needle insertions (70 insertions) were available for analysis.

The needle insertion forces inside the prostate mainly came from the tissue cutting and viscoelastic frictional forces. Under the same experimental conditions (needle geometry, insertion speed, etc.), the variation of the magnitude of the forces can be used as an indicator of tissue composi-
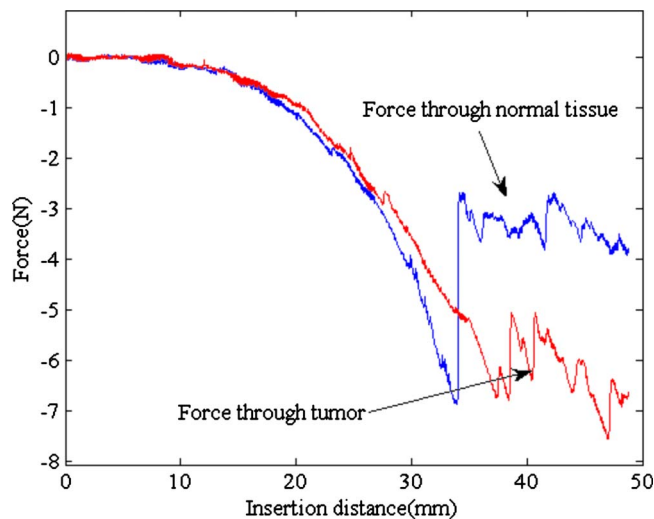
FIG. 4. An example of forces through normal tissue vs tumor.

TABLE I. Summary of mean forces through tumor vs normal tissues.

Groups	Tumor	Normal
Count	11	11
Mean	3.64	2.21
Variance	0.42	0.44
Standard deviation	0.64	0.66

ethnicity, prostate volume, prostate density, PSA level, and so on), which may contribute to the force variances.

III.B. Statistically significant patient-specific factors

A total of six iterations were performed using data from the 70 insertions until a model with only significant factors was obtained. The final result reveals that prostate density and PSA have significant effects on the mean forces. The p value less than 0.0001 suggests that the regression model is significant. The Durbin-Watson value at 1.94, being larger than 1.161, which is the cutoff value for two regressors (excluding the intercept) and 21-sample size,[18] indicates no autocorrelation. In the regression model, the force monotonically increases with density and PSA; this reveals that larger prostate density and higher PSA level tend to produce larger insertion forces. The relationships between needle insertion force and prostate density, as well as PSA, are used as constraints for the selection of the parameters during optimization, which will be discussed in Sec. II C.

III.C. Optimal baseline model with simulation results

The optimization engine has been implemented in MAT-LAB (MathWorks, Inc., MA). Experimental data from ten patients were selected for modeling. The selection of patients for model prediction was based on factorial design,[24] where the patient-specific factors in the selected modeling data set should cover the lowest and highest levels of the corresponding factors in the entire data set. Pathological data were used as ground truth to measure the correctness of the cancer detection method, from which sensitivity and specificity were computed. Previous regression study in Sec. III B has shown that the first-order linear model was sufficient for the current small data set (p value <0.0001). Thus the order of the baseline model (n_i) was set to be "1" for simplicity. In the future, with more data available, the order should also be optimized. In addition, the regression analysis indicates that the force monotonically increases with density and PSA. Therefore, the feasible domain for the parameters of both density and PSA was constrained to half Cartesian space, where the parameters had the same negative signs as the force. These two constraints were used in the optimization procedure.

The optimization algorithm was run with the parameter vector initialized at $[-0.10; -0.70; -0.10]$, which represented the constant and parameters of density and PSA, respectively. The resulting optimal parameter vector was $[-0.06; -0.06; -0.175]$, with which the maximum AUC was achieved at 0.80. As comparison, for a force model without patient-specific factors, the maximum AUC achievable

tion variability along the needle path. Figure 4 shows an example of needle insertion forces inside the normal tissue vs the tumor. As can be observed from the figure, the tumor required a larger force (compressive force is represented by negative sign) to pass through. Comparison of the absolute mean insertion forces through the cancerous tissue with those through the normal tissue revealed that the former was larger than the latter by 0.7–2.2 N (see Fig. 5), which could be explained by the increased hardness in the cancerous tissue.[12,16] In our 21 cases (70 insertions), only 11 cases (38 insertions) that had insertions passing through both the cancerous tissue and normal tissue were included for comparison. The mean forces of all the individual insertions passing through the same type of tissues (tumor and normal tissue) in the same patients were calculated and compared. Table I presents the statistical summary. The small p value (<0.01) obtained from analysis of variance (ANOVA) indicates that the force variance between the cancerous and normal tissues is significant. In addition, as shown in Fig. 5, the mean forces from different patients are shown to be different even in the same type of tissue. In Sec. III B, we investigated the statistically significant patient-specific factors (i.e., patient age,
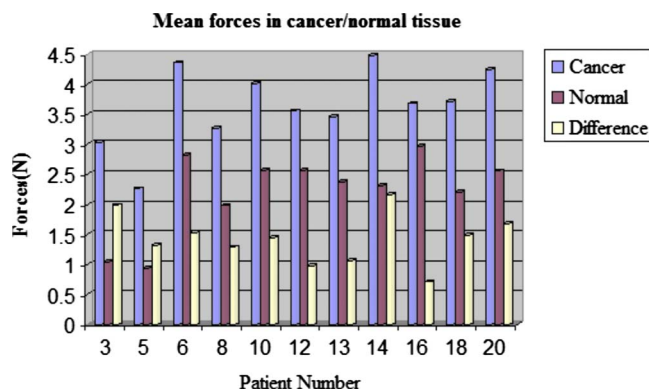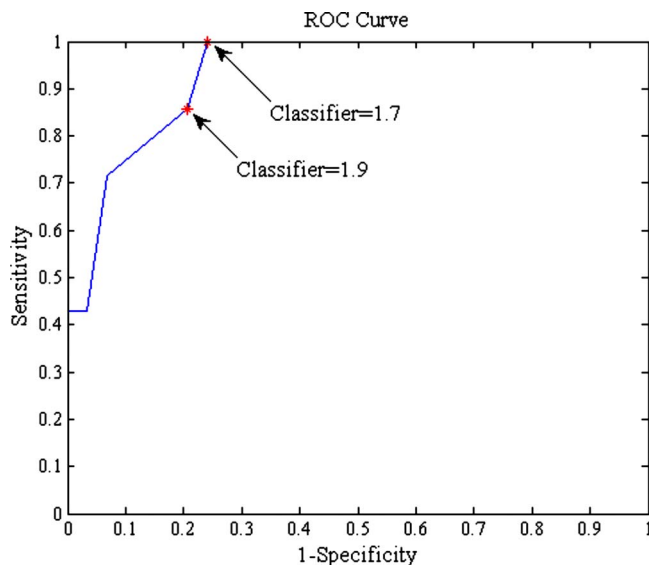

FIG. 5. Comparison of mean forces (absolute values) in the cancerous tissue and normal tissue at central zone.
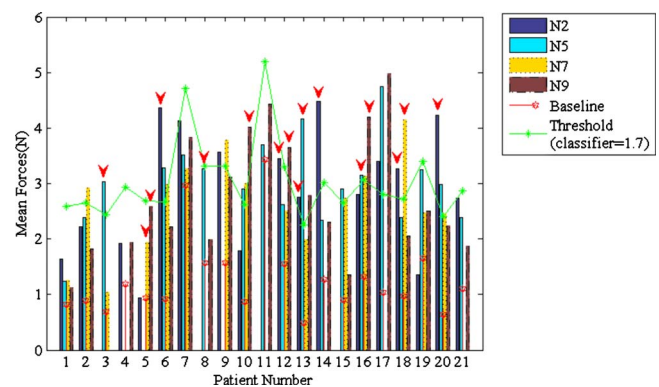
FIG. 6. ROC curve.

FIG. 7. Needle insertion forces in central zone of the prostate with generated baseline forces and thresholds using classifier 1.7. The arrows point to the ones with cancer.

was 0.55. Similarly, for a model with density or PSA only, the maximum AUCs achievable were 0.59 and 0.75, respectively. This demonstrates that characterizing the insertion force using the statistically significant factors will result in better estimation.

The model was then validated using the data of the remaining 11 patients. By varying the classifier values in increments of 0.2, an ROC curve was generated, as shown in Fig. 6. The AUC calculated using this independent set of validation data was equal to 0.90. With a classifier of 1.7, sensitivity of 100% and specificity of 76% can be achieved, while with a classifier of 1.9, sensitivity of 86% and specificity of 79% can be achieved. Figure 7 shows the absolute mean insertion forces in the central zone (N2, N5, N7, N9) for all 21 patients, together with the estimated baseline forces and the thresholds after applying a classifier of 1.7.

IV. DISCUSSIONS

As can be observed from Fig. 7, the majority of the cancers could be detected with a classifier of 1.7. Some false cancer detections resulted for the following reasons. First, the present baseline force model included two patient-specific factors: Prostate density and PSA values. Other factors such as the Gleason score and cancer stage may also have an influence on the force model. In the present small data set, these factors were not found to be statistically significant, probably due to the narrow variances of their values, as shown in Table II, thus resulting in insignificant changes in the corresponding forces. The use of a constant mean (-0.06) for the uncharacterized force part would result in errors in predicting the baseline force. The solution to improve the baseline force model would be to expand the study with more patients' data to further investigate and identify the statistically significant patient-specific factors.

Another reason for incorrect diagnoses may come from experimental procedure errors. For example, insertion forces in patient 17 were high due to significant prostate movement during needle insertion. Potential approaches to overcome this problem include better immobilization of the prostate specimens. In some other cases, high composition of the fibromuscular (FM) component ($\geq 80\%$) (e.g., N7 in patient 2) or occurrence of benign prostatic hyperplasia (BPH) (e.g., N9 in patient 17) would also result in higher insertion forces as compared to other insertions in the same patient, thus leading to the wrong diagnosis. A multimodal method that combines this technique with other tissue characterization techniques [e.g., ultrasound tissue characterization[25] or acoustic radiation force (ARF) sonocontrast technique[26]] may help improve cancer discrimination specificity.

One concern in applying the current model is how to estimate the prostate density *in vivo*. Some potential techniques could be via imaging methods, such as relying on carefully calibrated CT densities or replacing density with other similar, surrogate patient-specific criterion, e.g., tissue elasticity measured using imaging techniques,[27] which may be consid-

TABLE II. Summary of input data.

Group	Age	PSA	BMI	Gleason's score	Density	Volume	Ethnicity	Clinical stage
Count	21	21	18	21	21	21	20	21
Mean	62.58	6.52	29.22	6.29	0.61	108.09	*No. of patients*	
Variance	49.84	17.06	11.29	0.21	0.01	1158.04		
SD	7.06	4.13	3.36	0.46	0.11	34.03	Black:3	T1c: 17
							White:17	T2a: 4
%SD/mean	11.28	63.27	11.50	7.37	17.76	31.48		

ered in the future. One limitation of the proposed cancer detection methodology is that it can only detect tumor foci along the needle insertion trajectory.

In the current study, we had data of 21 patients, of which data of 10 patients were used for model construction and data of 11 patients were used for model validation. For the modeling set, the mean force is -2.92 N with a standard deviation (SD) of 1.12 N, and there are nine cancers in the data set, while for the testing set, the mean force is -2.74 N with a standard deviation of 0.77 N, and there are seven cancers in the data set. Wilcoxon rank sum test[28] of the two data sets for equal medians gave a p value of 0.90, which suggests that the two independent data sets come from identical distributions. This demonstrates that the selection of the data sets is not biased. Additional patient data will be helpful for better "training" of the baseline force model and further evaluating the proposed methodology. We classified the whole prostate into three (peripheral, central, and transitional) zones and intended to build a model for each zone separately. Due to insufficient number of successful insertions passing through both tumor and normal tissue in the peripheral and transitional zones, only forces in the central zone were studied. The other two zones, especially the peripheral zone where most cancers tend to develop, will be studied in the future. Also in the current model, only patient-specific factors were included. Procedure-related factors (needle insertion speed, insertion depth, needle size, etc.) were not included. In the future, we will use different types of needles with various insertion speeds and improve prostate specimen immobilization, so that the procedure-related factors can be included in the model.

V. CONCLUSIONS

In this paper, a novel approach for real-time cancer detection using needle insertion force has been presented. After parameter optimization using data from 10 patients, the technique achieved an AUC of 0.90 when evaluated using an independent set of validation data from another 11 patients. The feasibility of cancer detection in real time during interstitial interventions is established. The proposed technique is intended to be used in robotic brachytherapy with real-time force sensing and dynamic planning to achieve targeted therapy. Other potential applications include biopsy, photodynamic therapy, and thermal ablation.

ACKNOWLEDGMENT

a)Author to whom correspondence should be addressed. Electronic mail: kaiguo.yan@jeffersonhospital.org; Telephone: (215)-955-6043; Fax: (215)-955-0412.

1NCI website: http://www.cancer.gov/cancertopics/types/prostate, accessed in July 2008.

2P. N. Brett, T. J. Parker, A. J. Harrison, T. A. Thomas, and A. Carr, "Simulation of resistance forces acting on surgical needles," Proc. Inst. Mech. Eng., Part H: J. Eng. Med. **211**, 335–347 (1997).

3T. K. Podder *et al.*, "Method to reduce force and target movement during surgical needle interventions," Proceedings of the Third European Medical & Biological Engineering Conference (EMBEC), Prague, Czech Republic, 2005, Vol. 11, pp. 4315–4320.

4A. M. Okamura, C. Simone, and M. D. O'Leary, "Force modeling for needle insertion into soft tissue," IEEE Trans. Biomed. Eng. **51**, 1707–1716 (2004).

5J. T. Hing, A. D. Brooks, and J. P. Desai, "Reality based needle insertion simulation for haptic feedback in prostate brachytherapy," Proceedings of the IEEE International Conference on Robotics and Automation, 2006, pp. 619–624.

6T. Hu, J. P. Desail, A. Castellanos, and A. Lau, "Modeling in vivo soft tissue probing," Proceedings of the First IEEE/RAS-EMBS International Conference on Biomedical Robotics and Biomechatronics, Pisa, Italy, 2006, pp. 537–542.

7T. K. Podder *et al.*, "In vivo motion and force measurement of surgical needle intervention during prostate brachytherapy," Med. Phys. **33**, 2915–2922 (2006).

8T. K. Podder *et al.*, "Effects of velocity modulation during surgical needle insertion," Proceedings of the IEEE EMBS, Shanghai, China, 2005, pp. 5766–5770.

9K. Yan *et al.*, "A novel method for estimating needle insertion force using patient-specific factors," Int. J. CARS **3**, 165–166 (2008).

10T. K. Podder *et al.*, "Needle insertion force estimation model using procedure-specific and patient-specific criteria," Proceedings of the 28th IEEE EMBS Annual International Conference, New York, NY, 2006, pp. 555–558.

11N. Abolhassani, R. Patel, and M. Moallema, "Needle insertion into soft tissue: A survey," Med. Eng. Phys. **29**, 413–431 (2007).

12V. Jalkanen, B. M. Andersson, A. Bergh, B. Ljungberg, and O. A. Lindahl, "Prostate tissue stiffness as measured with a resonance sensor system: A study on silicone and human prostate tissue in vitro," Med. Biol. Eng. Comput. **44**, 593–603 (2006).

13V. Jalkanen, Ph.D. thesis, Umeå University, Umeå, Sweden, 2006.

14L. S. Taylor, J. Tamez-Pena, J. S. Smith, D. Rubens, and K. J. Parker, "3D sonoelastography for visualization of tumors," Proceedings of the IEEE Ultrasonics Symposium, 1997, pp. 1443–1446.

15L. S. Taylor, B. C. Porter, D. J. Rubens, and K. J. Parker, "Three-dimensional sonoelastography: Principles and practices," Phys. Med. Biol. **45**, 1477–1494 (2000).

16L. S. Taylor, M. S. Richards, and A. J. Moskowitz, "Viscoelastic effects in sonoelastography: Impact on tumor detectability," Proceedings of the IEEE Ultrasonics Symposium, 2001, pp. 1639–1642.

17C. T. Haan, *Statistical Methods in Hydrology*, 2nd ed. (Iowa State University Press, Ames, IA, 2002).

18J. Durbin and G. S. Watson, "Testing for serial correlation in least squares regression, II," Biometrika **38**, 159–179 (1951).

19M. Gaviano and F. Testa, "A general convergence theorem for the reduced gradient method," Numer. Math. **43**, 241–247 (1984).

20I. M. Nejdawi, K. A. Clements, and P. W. Davis, "An efficient interior point method for sequential quadratic programming based optimal power flow," IEEE Trans. Power Syst. **15**, 1179–1183 (2000).

21G. Di Pillo and L. Grippo, "An augmented Lagrangian for inequality constraints in nonlinear programming problems," J. Optim. Theory Appl. **36**, 495–519 (1982).

22R. Fletcher, *Practical Methods of Optimization* (Wiley, New York, 1987).

23S. P. Han, "A globally convergent method for nonlinear programming," J. Optim. Theory Appl. **22**, 297–309 (1977).

24D. C. Montgomery, *Design and Analysis of Experiments* (Wiley, New York, 1997).

25T. Liu, F. L. Lizzi, R. H. Silverman, and G. J. Kutcher, "Ultrasonic tissue characterization using 2D spectrum analysis and its application in ocular tumor diagnosis," Med. Phys. **31**, 1032–1039 (2004).

26B. A. Winey, V. Misic, L. Liao, K. Parker, B. Fenton, and Y. Yu, "In vivo cancer diagnosis with optical spectroscopy and acoustically induced blood stasis using a murine MCa35 model," Med. Phys. **33**, 1623–1633 (2006).

27L. Pallwein *et al.*, "Real-time elastography for detecting prostate cancer: Preliminary experience," BJU Int. **100**, 42–46 (2007).

28J. D. Gibbons, *Nonparametric Statistical Inference*, 2nd ed. (Dekker, New York, 1985).